Society of Medical Education & Research

2022, Volume 2, Issue 2, Page No: 143-163
ISSN: 3108-4834

Archive of International Journal of Cancer and Allied Science

Fucosylated Exosomal miR-6842-3p from Cancer Cells Drives Angiogenesis and Metastasis in ESCC through the PTEN/AKT/mTOR/IRF1/CXCL10 Signaling Pathway and Serves as a Novel Biomarker

Johanna Christina Petersen[1]*, Frederik Henrik Larsen[1]

[1]Department of Oncology, Rigshospitalet, University of Copenhagen, Copenhagen, Denmark.

***E-mail** ✉ j.petersen.rigs@outlook.com

Abstract

Tumor-derived fucosylated exosomes (FUC-Exo) have emerged as critical contributors to cancer progression, yet the roles and mechanisms of exosomal fucosylated miRNAs in esophageal squamous cell carcinoma (ESCC) remain largely unexplored. By employing lentil lectin (LCA)-coated magnetic beads to isolate FUC-Exo, followed by small RNA sequencing and RT-qPCR, miR-6842-3p was identified as a novel biomarker for ESCC. Functional studies in vitro and in vivo demonstrated its oncogenic and pro-angiogenic effects. Mechanistic investigations using dual-luciferase reporter assays, ChIP-qPCR, western blotting, and rescue experiments revealed the underlying pathways. miR-6842-3p is markedly elevated in ESCC tissues and serum FUC-Exo, correlates with advanced disease stages, poorer prognosis, and holds promise as an early diagnostic marker. Functioning as an oncogene, miR-6842-3p enhances tumor growth, metastasis, and angiogenesis. Upon uptake by HUVECs, tumor-derived fucosylated exosomal miR-6842-3p suppresses PTEN, leading to AKT and mTOR phosphorylation, subsequent downregulation of IRF1, decreased CXCL10 expression, and ultimately enhanced angiogenesis. These findings establish miR-6842-3p as a pivotal regulator of ESCC progression and angiogenesis, with fucosylated exosomal miR-6842-3p acting through the PTEN/AKT/mTOR/IRF1/CXCL10 axis, underscoring its potential as both a biomarker and therapeutic target in ESCC.

Keywords: miR-6842-3p, Cancer cells, Biomarker, Exosomal

Introduction

Oesophageal squamous cell carcinoma (ESCC) is a major contributor to global cancer morbidity, especially in East Asia, where it represents roughly 90% of all esophageal cancer cases [1]. Despite advances in treatment strategies, the prognosis remains poor, with a five-year survival rate below 20% [2], emphasizing the critical need for early detection and the development of targeted therapies to improve patient outcomes.

Access this article online https://smerpub.com/

Received: 09 September 2022; **Accepted:** 06 December 2022

How to cite this article: Petersen JC, Larsen FH. Fucosylated Exosomal miR-6842-3p from Cancer Cells Drives Angiogenesis and Metastasis in ESCC through the PTEN/AKT/mTOR/IRF1/CXCL10 Signaling Pathway and Serves as a Novel Biomarker. Arch Int J Cancer Allied Sci. 2022;2(2):143-63. https://doi.org/10.51847/tnlPchqRVI

The tumor microenvironment (TME) is increasingly recognized as a key determinant of ESCC progression. Tumor-derived exosomes, as nanoscale vesicles facilitating intercellular communication, play crucial roles by transferring bioactive molecules such as miRNAs, thereby influencing proliferation, metastasis, angiogenesis, and epithelial-mesenchymal transition (EMT) [3–5]. Among post-translational modifications, abnormal glycosylation, particularly fucosylation, has been implicated in tumor progression [6, 7]. Fucosylation involves the addition of fucose residues to glycoproteins or glycolipids and affects processes such as cell adhesion, signal transduction, and immune escape [6].

Exosomes, 40–150 nm in diameter, originate from endosomal compartments and mediate intercellular signaling by delivering proteins, lipids, and nucleic acids to recipient cells [8]. Their surface glycosylation, particularly fucosylation mediated by

fucosyltransferases, is critical for exosome stability, cellular uptake, and cargo delivery efficiency [9]. Exosomes with elevated surface fucosylation—termed fucosylated exosomes (FUC-Exo)—have emerged as important modulators of tumor behavior [7]. Enhanced fucosylation in cancer cells often leads to increased secretion of FUC-Exo, making them a unique subset of exosomes that can provide valuable insights into tumor initiation and progression [10].

Our prior studies using small RNA sequencing and RT-qPCR revealed that miR-6842-3p is significantly enriched in serum FUC-Exo from ESCC patients compared with healthy controls [11]. Preliminary functional assays indicated that exosomal miR-6842-3p promotes proliferation, invasion, and migration of ESCC cells [11]. Nevertheless, the specific contribution of fucosylated exosomal miR-6842-3p to TME remodeling, its underlying molecular mechanisms, and its clinical relevance remain poorly characterized. Investigating these aspects may uncover its potential as a prognostic biomarker and therapeutic target.

In this study, building on our previous work, we demonstrate that miR-6842-3p in serum FUC-Exo is a promising early diagnostic marker for ESCC, with high expression correlating with reduced patient survival. Mechanistically, we reveal that tumor-derived fucosylated exosomal miR-6842-3p fosters a pro-metastatic microenvironment via a signaling axis involving PTEN, AKT, mTOR, IRF1, and CXCL10. These findings provide novel insights into how fucosylated exosomal miRNAs regulate angiogenesis and metastasis, establishing their potential as both biomarkers and therapeutic targets in ESCC management.

Results and Discussion

Fucosylated exosomal miR-6842-3p exhibits diagnostic potential in ESCC

To investigate the role of fucosylated exosomal miRNAs in ESCC progression, we implemented a five-step strategy encompassing biomarker discovery, screening, training, internal validation, and external validation **(Figure 1a)**. This multi-phase approach identified four miRNAs—miR-1228-5p, miR-6842-3p, miR-30e-3p, and miR-642a-3p—as significantly upregulated in serum FUC-Exo from ESCC patients compared to healthy controls, whereas their expression in total exosomes showed no significant difference [11]. Since miR-1228-5p, miR-30e-3p, and miR-642a-3p have been extensively investigated in other cancers [12–14], we focused on the relatively uncharacterized miR-6842-3p.

Through systematic validation, we confirmed that fucosylated exosomal miR-6842-3p possesses strong diagnostic potential for ESCC, achieving AUC values of 0.888 in the screening cohort, 0.916 in the training cohort, 0.870 in internal validation, and 0.862 in external validation, outperforming conventional serum markers SCC-Ag and CEA **(Figure 1b)**. Notably, miR-6842-3p levels were significantly elevated in early-stage ESCC patients compared with healthy controls, indicating its utility for early detection (AUC = 0.908 in the training cohort; AUC = 0.875 in external validation), outperforming CEA **(Figure 1e)**.

Furthermore, increased serum FUC-Exo miR-6842-3p was strongly associated with advanced disease stages ($p = 0.019$ in the training cohort, **(Table 1)**; $p = 0.037$ in external validation) and correlated with poor prognosis ($p < 0.01$; HR = 2.165) in the training cohort **(Table 1 and Figure 1f)**. Consistent with serum results, miR-6842-3p expression was significantly higher in ESCC tissues than in adjacent normal tissues (n = 40) **(Figure 1g)**. Collectively, these findings highlight the value of serum fucosylated exosomal miR-6842-3p as both an early diagnostic and prognostic biomarker, emphasizing its potential functional role in ESCC progression.

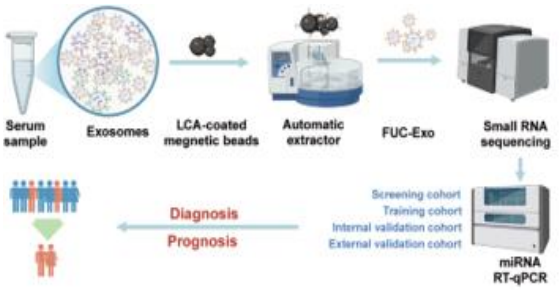

a)

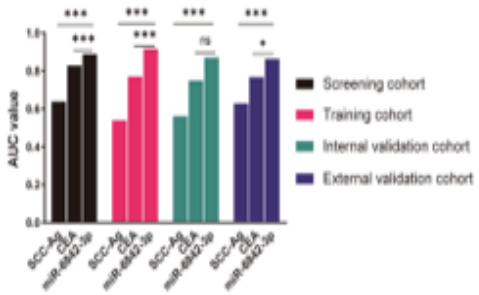

b)

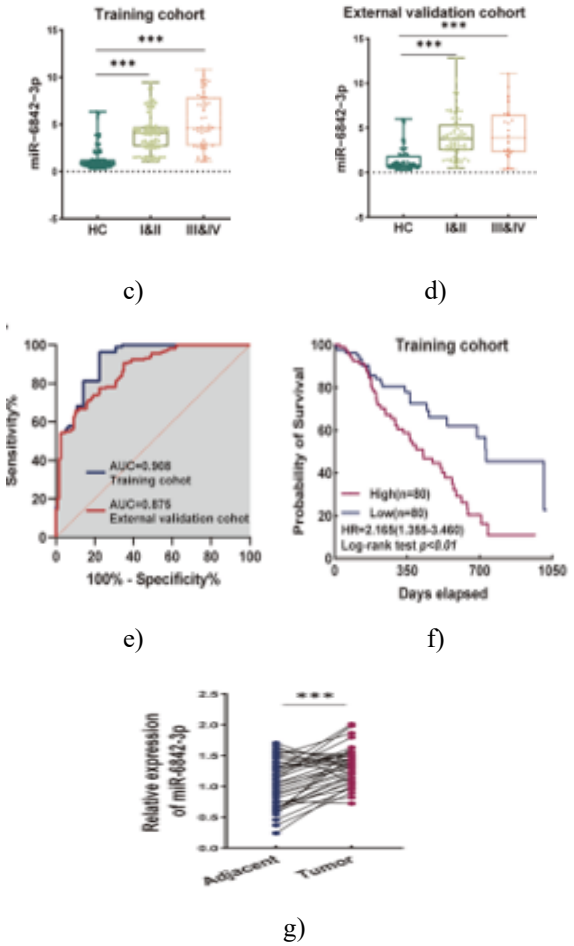

Figure 1. Assessment of fucosylated exosomal miR-6842-3p as a diagnostic and prognostic indicator in ESCC.

(a) Schematic outline illustrating the sequential strategy used for candidate miRNA identification, screening, and validation. LCA denotes lentil lectin.

(b) Receiver operating characteristic (ROC) curve analysis comparing the diagnostic accuracy of fucosylated exosomal miR-6842-3p with conventional serum markers SCC-Ag and CEA across multiple cohorts: screening (24 HCs vs. 24 ESCC), training (120 HCs vs. 160 ESCC), internal validation (45 HCs vs. 60 ESCC), and external validation (72 HCs vs. 105 ESCC). Differences between ROC curves were evaluated using DeLong's test; nsp > 0.05, *p < 0.05, ***p < 0.001; HC, healthy control.

(c–d) Serum levels of fucosylated exosomal miR-6842-3p stratified by tumor stage. Data are shown for the training cohort (C: 120 HCs vs. 107 stage I&II ESCC, 120 HCs vs. 53 stage III&IV ESCC) and the external validation cohort (D: 72 HCs vs. 80 stage I&II ESCC, 72 HCs vs. 25 stage III&IV ESCC). Results are presented as mean ± SEM and analyzed using the Kruskal–Wallis test followed by Dunnett's multiple-comparison test; ***p < 0.001.

(e) ROC analysis demonstrating the ability of fucosylated exosomal miR-6842-3p to distinguish early-stage (I&II) ESCC from healthy controls in the training cohort, with confirmation in the external validation cohort.

(f) Kaplan–Meier survival curves for ESCC patients in the training cohort, categorized into high- and low-expression groups based on the median level of serum fucosylated exosomal miR-6842-3p. Survival differences were assessed using the log-rank test, with p < 0.05 considered statistically significant.

(g) Comparison of miR-6842-3p expression between ESCC tumor tissues and matched adjacent noncancerous tissues (n = 40 pairs). Data are expressed as mean ± SEM, and statistical significance was determined using a paired Student's t-test; ***p < 0.001.

Table 1. Association between serum fucosylated exosomal miR-6842-3p expression and clinicopathological features in the training cohort

Clinicopathological parameter	miR-6842-3p High expression (n = 80, 50%)a	Total cases (n = 160)a	miR-6842-3p Low expression (n = 80, 50%)a	p-valueb	χ^2 value
Age (years)				0.635	0.23
> 60	40 (50.00%)	84 (52.50%)	44 (55.00%)		
≤ 60	40 (50.00%)	76 (47.50%)	36 (45.00%)		
Sex				0.269	1.22
Female	16 (20.00%)	39 (24.38%)	23 (28.75%)		
Male	64 (80.00%)	121 (75.63%)	57 (71.25%)		

Primary tumor depth (T stage)				0.170	1.88
T1/T2	51 (63.75%)	111 (69.38%)	60 (75.00%)		
T3/T4	29 (36.25%)	49 (30.63%)	20 (25.00%)		
Lymph node involvement				0.154	2.04
Absent	17 (21.25%)	43 (26.88%)	26 (32.50%)		
Present	63 (78.75%)	117 (73.13%)	54 (67.50%)		
Clinical stage				0.019	5.53
Stage I–II	46 (57.50%)	107 (66.88%)	61 (76.25%)		
Stage III–IV	34 (42.50%)	53 (33.13%)	19 (23.75%)		
Histopathological grade				0.095	2.80
Poorly differentiated	24 (30.00%)	38 (23.75%)	14 (17.50%)		
Well/Moderately differentiated	56 (70.00%)	122 (76.25%)	66 (82.50%)		

a Data are presented as number (%).

b Statistical significance was evaluated using Pearson's chi-squared test.

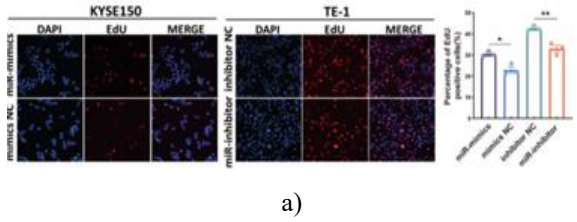

a)

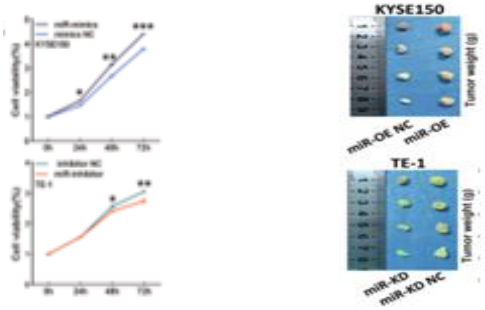

b) g)

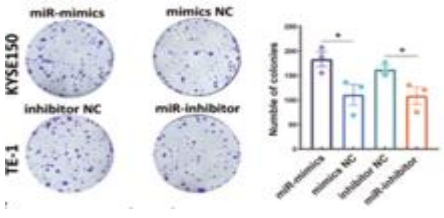

c)

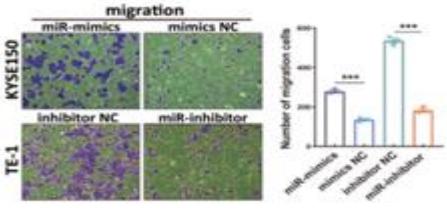

d)

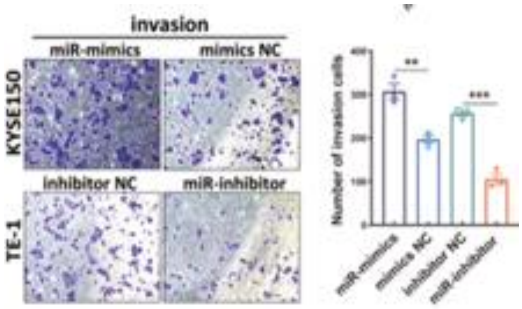

e)

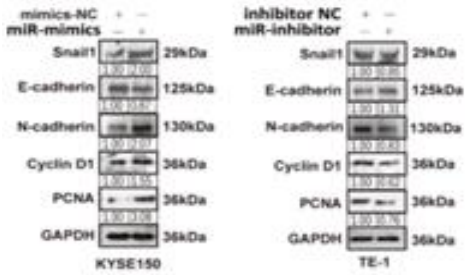

f)

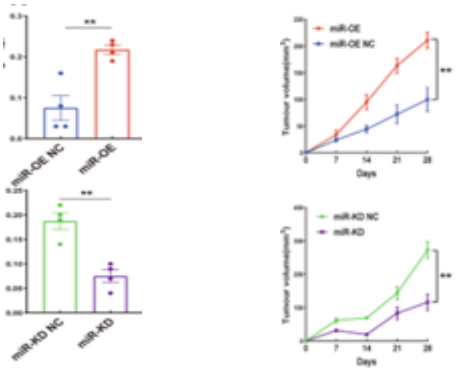

h) i)

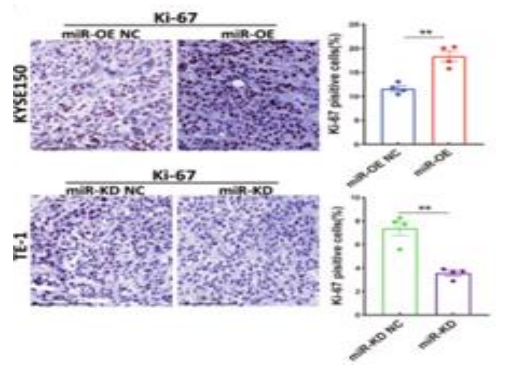

j)

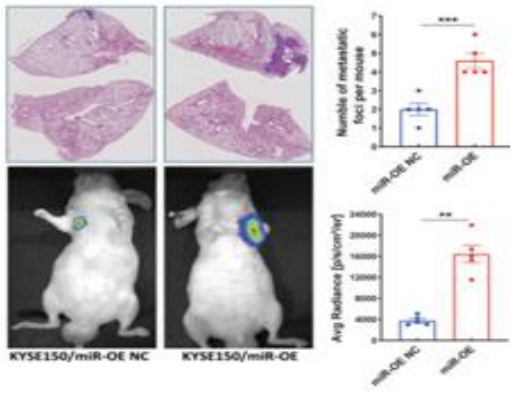

k)

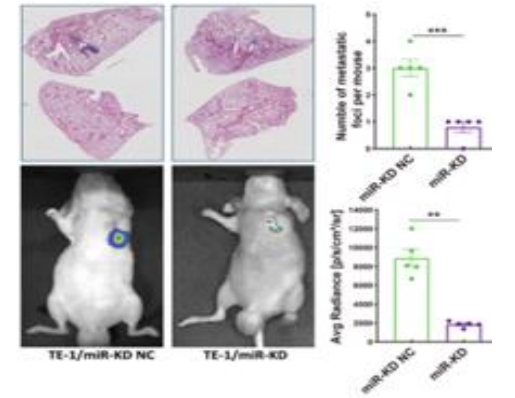

k)

Figure 2. Functional characterization of miR-6842-3p in regulating ESCC proliferation, motility, EMT, and tumor progression in vitro and in vivo.
(a–c) Cell growth was assessed in ESCC cells following transfection with miR-6842-3p mimics or inhibitors using EDU incorporation (a; scale bar, 100 μm), CCK-8 metabolic activity assay (b), and clonogenic assays (c; scale bar, 50 μm). Data are shown as mean ± SEM from three independent experiments; *p < 0.05, **p < 0.01, ***p < 0.001.
(d–e) Transwell-based assays were employed to evaluate changes in migratory (d) and invasive (e) behavior after miR-6842-3p modulation, with Matrigel coating used for invasion assays. Representative images are shown (scale bar, 100 μm). Results are presented as mean ± SEM (n = 3); **p < 0.01, ***p < 0.001.
(f) Immunoblot analysis of EMT-associated proteins (Snail1, E-cadherin, and N-cadherin) and proliferation-related markers (Cyclin D1 and PCNA) in ESCC cells transfected with miR-6842-3p mimics or inhibitors. Protein expression levels were quantified relative to GAPDH.
(g–i) In vivo tumorigenicity assays using nude mouse xenograft models generated from KYSE150 cells (miR-OE NC or miR-OE) and TE-1 cells (miR-KD NC or miR-KD). Representative tumor images (g), tumor weights (h), and tumor growth curves (i) are shown. Values represent mean ± SEM (n = 4); **p < 0.01.
(j) Immunohistochemical staining of xenograft tumors for the proliferation marker Ki-67, with quantitative analysis of positively stained cells (n = 4); **p < 0.01.
(k–l) Representative hematoxylin and eosin (H&E) staining of lung tissues showing metastatic lesions in the indicated groups. Metastatic burden was quantified using an in vivo imaging system (IVIS) based on total fluorescence intensity of whole lungs (n = 5); **p < 0.01, ***p < 0.001.

To corroborate the in vitro observations, we next evaluated the oncogenic activity of miR-6842-3p using in vivo models. KYSE150 cells stably expressing Lv-miR-6842-3p-mimic (miR-OE) and TE-1 cells carrying Lv-miR-6842-3p-inhibitor constructs (miR-KD) were successfully established, as confirmed by RT-qPCR. In subcutaneous xenograft experiments, tumors derived from miR-OE cells displayed markedly accelerated growth, characterized by increased tumor volume and mass compared with their corresponding control group. In contrast, suppression of miR-6842-3p in TE-1 cells resulted in significantly reduced tumor growth relative to controls **(Figures 2g–2i)**.
Consistent with these findings, immunohistochemical analysis revealed enhanced Ki-67 staining in miR-OE-derived tumors, whereas tumors formed from miR-KD cells exhibited a substantial reduction in Ki-67-positive cells, indicating diminished proliferative activity **(Figure 2j)**. Moreover, lung metastasis assays demonstrated that enforced miR-6842-3p expression

markedly increased metastatic dissemination, as evidenced by a higher number of pulmonary metastatic foci, while miR-6842-3p inhibition significantly restrained metastatic colonization **(Figures 2k and 2l)**. Collectively, these in vivo results confirm that miR-6842-3p acts as a potent promoter of ESCC tumor growth and metastatic progression.

miR-6842-3p directly suppresses PTEN, activates AKT signaling, and facilitates ESCC proliferation and metastasis

To identify downstream effectors mediating the oncogenic functions of miR-6842-3p in ESCC, we integrated five independent miRNA–mRNA prediction platforms (miRTarBase, miRWalk, miRDB, RNA22, and RNAInter) to systematically screen potential target genes. This comprehensive analysis yielded 13 candidate mRNAs **(Figure 3a)**, among which seven were annotated as tumor suppressors. Subsequent RT-qPCR validation revealed that all seven tumor suppressor genes were significantly repressed in KYSE150 cells following miR-6842-3p overexpression, with PTEN exhibiting the most pronounced reduction in expression **(Figure 3b)**. Given the established role of PTEN as a central tumor suppressor across multiple malignancies [15], we selected PTEN for further mechanistic investigation.

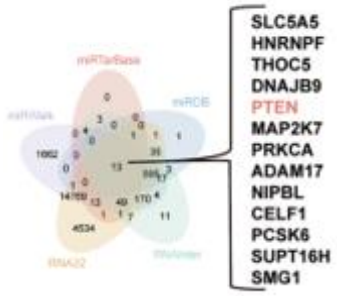

a)

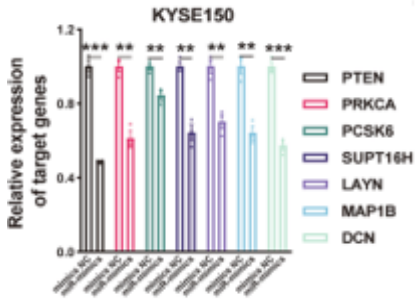

b)

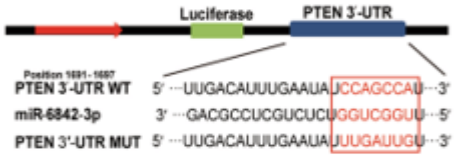

c)

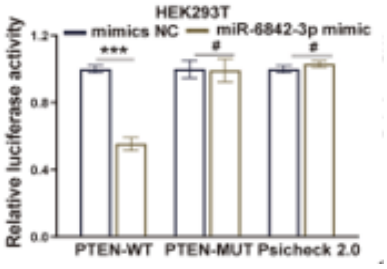

d)

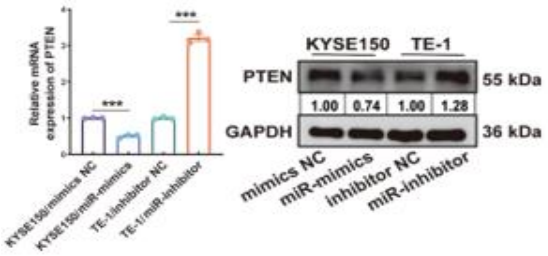

e)

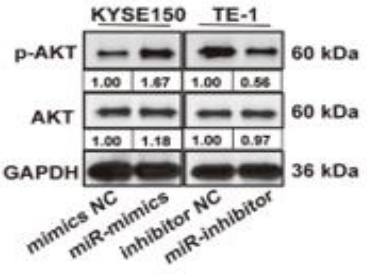

f)

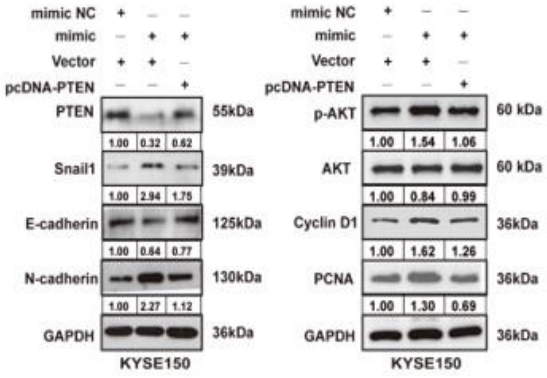

g)

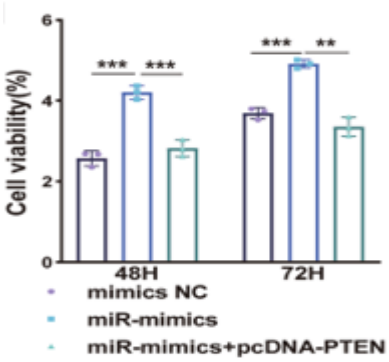

h)

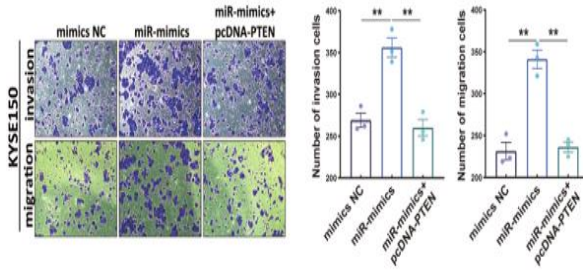

i)

Figure 3. miR-6842-3p directly represses PTEN, triggers AKT pathway activation, and enhances ESCC proliferative and metastatic phenotypes.

(a) A Venn diagram illustrates the intersection of predicted miR-6842-3p target genes identified using miRTarBase, miRWalk, miRDB, RNA22, and RNAInter.

(b) RT-qPCR-based screening of candidate target genes in KYSE150 cells transfected with miR-6842-3p mimics or mimic NC; data are shown as mean ± SEM (n = 3), **p < 0.01, ***p < 0.001.

(c) Schematic depiction of the dual-luciferase reporter plasmid containing the PTEN 3′UTR, with the miR-6842-3p seed-binding site highlighted.

(d) Quantification of relative luciferase activity in the indicated groups determined by dual-luciferase reporter assays; values represent mean ± SEM (n = 3), #p > 0.05, ***p < 0.001.

(e) RT-qPCR and western blot analyses showing PTEN mRNA and protein expression in ESCC cells following miR-6842-3p overexpression or inhibition; mean ± SEM, ***p < 0.001.

(f) Immunoblot analysis of total AKT and phosphorylated AKT (p-AKT) in ESCC cells subjected to miR-6842-3p gain- or loss-of-function.

(g) Western blot detection of PTEN, EMT-associated markers (Snail1, E-cadherin, N-cadherin), AKT signaling components, and proliferation-related proteins (Cyclin D1 and PCNA) in KYSE150 cells under the indicated treatments.

(h) CCK-8 assays assessing cell proliferation in KYSE150 cells with quantitative analysis; mean ± SEM (n = 3), **p < 0.01, ***p < 0.001.

(i) Transwell migration and invasion assays performed in KYSE150 cells, followed by statistical quantification; mean ± SEM (n = 3), **p < 0.001.

Note: Protein expression levels were normalized to GAPDH for densitometric quantification.

To validate PTEN as a direct downstream effector of miR-6842-3p, luciferase reporter assays were conducted in HEK293T cells. miR-6842-3p markedly suppressed reporter activity driven by the wild-type PTEN 3′UTR, whereas mutation of the predicted binding site abolished this effect **(Figures 3c and 3d)**. Consistently, RT-qPCR and western blot analyses demonstrated that enforced miR-6842-3p expression significantly reduced PTEN abundance in KYSE150 cells, while miR-6842-3p inhibition led to increased PTEN expression in TE-1 cells **(Figure 3e).**

PTEN is a well-established upstream inhibitor of AKT signaling, and its functional loss commonly results in AKT activation across multiple malignancies [16, 17]. In line with this paradigm, western blot analysis revealed that miR-6842-3p overexpression decreased PTEN levels and simultaneously elevated p-AKT in KYSE150 cells. In contrast, miR-6842-3p silencing restored PTEN expression and reduced AKT phosphorylation in TE-1 cells **(Figures 3e and 3f)**.

To determine whether miR-6842-3p-mediated oncogenic effects were dependent on PTEN suppression, rescue experiments were performed. Restoration of PTEN expression counteracted miR-6842-3p-induced increases in p-AKT, reversed EMT-associated protein alterations, and normalized the expression of proliferation markers **(Figure 3g)**. Functionally, PTEN reintroduction significantly mitigated miR-6842-3p-driven cell proliferation, as shown by CCK-8 assays **(Figure 3h)**, and substantially reduced the enhanced migratory and invasive capabilities induced by miR-6842-3p mimics in KYSE150 cells **(Figure 3i)**. Collectively, these findings demonstrate that miR-6842-3p promotes ESCC growth and metastatic behavior by directly targeting PTEN and activating AKT signaling.

ESCC cells preferentially package miR-6842-3p into fucosylated exosomes, enabling endothelial uptake and intercellular transfer

Given the pivotal role of angiogenesis in metastatic dissemination and mounting evidence linking exosomal miRNAs to tumor-driven vascular remodeling [18], we next investigated whether miR-6842-3p participates in angiogenic regulation via fucosylated exosome-mediated transport. RT-qPCR analysis revealed that miR-6842-3p expression was significantly higher in ESCC cell lines (KYSE150, KYSE140, and TE-1) compared with HUVECs. KYSE150 and TE-1 cells, which exhibited relatively elevated miR-6842-3p levels, were therefore selected for subsequent experiments.

Fucosylated exosomes isolated from ESCC cell-conditioned media were characterized using transmission electron microscopy, nanoparticle tracking analysis, and western blotting **(Figures 4a and 4b)**. Stable miR-6842-3p-overexpressing KYSE150 and TE-1 cell lines were then established. RT-qPCR confirmed that miR-6842-3p upregulation in ESCC cells resulted in a corresponding increase in miR-6842-3p levels within both donor cells and their secreted fucosylated exosomes **(Figures 4c and 4d)**, indicating selective enrichment into tumor-derived FUC-Exo.

Upon exposure of HUVECs to fucosylated exosomes derived from miR-6842-3p-overexpressing ESCC cells, intracellular miR-6842-3p levels increased in a time-dependent manner, suggesting efficient exosomal uptake and transfer **(Figure 4e)**. This process was further validated by exosome internalization assays, in which WisTracker-labeled fucosylated exosomes originating from FAM-tagged miR-6842-3p-overexpressing KYSE150 or TE-1 cells were readily detected within HUVECs **(Figure 4f)**. Together, these results demonstrate that ESCC cells selectively load miR-6842-3p into fucosylated exosomes, which are subsequently internalized by endothelial cells to facilitate intercellular communication.

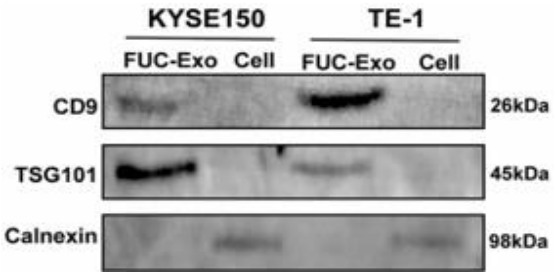

a)

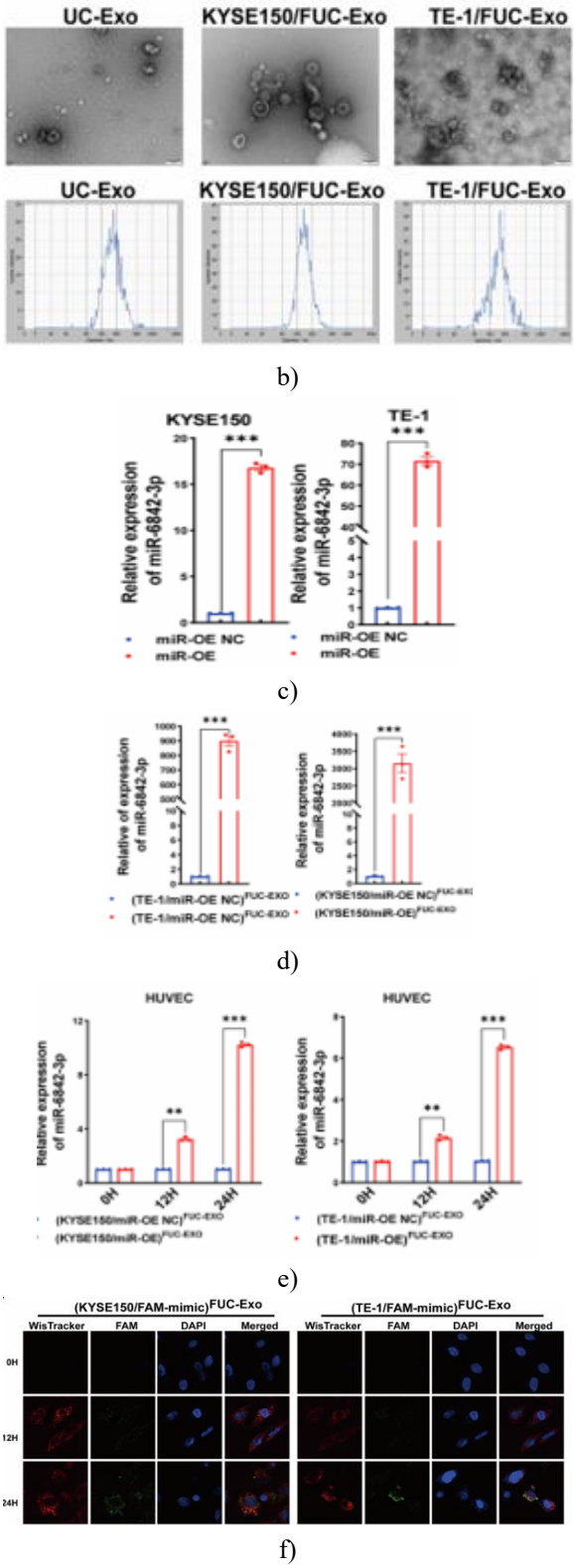

Figure 4. Tumour-derived fucosylated exosomes mediate the delivery of miR-6842-3p to HUVECs. (a) Western blotting confirmed the presence of canonical exosomal proteins (TSG101 and CD9) and

the absence of the endoplasmic reticulum marker Calnexin.

(b) Transmission electron microscopy and nanoparticle tracking analysis characterized the morphology and size distribution of fucosylated exosomes isolated from the conditioned media of KYSE150 and TE-1 cells (scale bar = 100 nm).

(c, d) RT-qPCR quantification of miR-6842-3p levels in KYSE150 and TE-1 cells following miR-6842-3p overexpression (miR-OE NC vs. miR-OE) and in their corresponding fucosylated exosomes; results are shown as mean ± SEM (n = 3), ***p < 0.001.

(e) Temporal assessment of miR-6842-3p accumulation in HUVECs exposed to fucosylated exosomes derived from control or miR-6842-3p-overexpressing ESCC cells for 0, 12, and 24 h; data represent mean ± SEM (n = 3), **p < 0.01, ***p < 0.001.

(f) Fluorescence microscopy images showing internalization of WisTracker-labeled fucosylated exosomes (red) originating from FAM-labeled miR-6842-3p-expressing KYSE150 or TE-1 cells (green) by HUVECs (scale bar = 10 μm).

miR-6842-3p-enriched fucosylated exosomes derived from ESCC cells stimulate angiogenesis and tumor progression

To explore the functional significance of miR-6842-3p in endothelial biology, HUVECs were transiently transfected with miR-6842-3p mimics or inhibitors, and effective modulation of miR-6842-3p expression was confirmed by RT-qPCR. Functional angiogenesis assays revealed that enforced miR-6842-3p expression markedly increased the formation of capillary-like networks, whereas miR-6842-3p suppression significantly impaired tube formation capacity.

Consistent with these observations, western blot analysis demonstrated that miR-6842-3p overexpression elevated the abundance of proteins associated with cell proliferation and angiogenesis, including MMP2, CD31, PCNA, and Cyclin D1, while simultaneously reducing the expression of endothelial tight junction components Occludin, ZO-1, and Claudin5; inverse effects were observed upon miR-6842-3p inhibition.

To substantiate these findings in vivo, HUVECs stably expressing miR-6842-3p or miR-6842-3p knockdown constructs were generated, with miRNA levels validated by RT-qPCR. Matrigel plug assays revealed a substantial increase in vascular infiltration within plugs containing miR-6842-3p-overexpressing cells, whereas miR-6842-3p depletion resulted in markedly reduced neovascularization. Furthermore, immunohistochemical staining of xenograft tumor sections showed elevated CD31 expression in miR-OE tumors and decreased CD31 positivity in miR-KD tumors relative to their respective controls, supporting a pro-angiogenic role for miR-6842-3p.

To determine whether the angiogenic effects of miR-6842-3p depend on fucosylated exosome-mediated transfer, KYSE150 miR-OE cells were treated with the exosome secretion inhibitor GW4869 prior to exosome isolation. Fucosylated exosomes collected from (miR-OE NC), (miR-OE), and (miR-OE + GW4869) groups were subsequently applied to HUVECs. RT-qPCR analysis demonstrated that exposure to (miR-OE) FUC-Exo significantly elevated intracellular miR-6842-3p levels in HUVECs, whereas this increase was effectively abolished following GW4869 pretreatment **(Figure 5a)**, indicating that miR-6842-3p transfer relies on active exosome release.

Functional assays further revealed that fucosylated exosomes derived from miR-6842-3p-overexpressing ESCC cells substantially enhanced HUVEC proliferation and migratory behavior, as assessed by EDU incorporation, transwell migration, and wound-healing assays. Notably, these effects were largely reversed when exosome secretion was inhibited by GW4869 **(Figures 5b–5d)**. Immunofluorescence staining demonstrated that (miR-OE) FUC-Exo disrupted endothelial tight junction integrity, whereas GW4869 treatment restored junctional protein expression **(Figure 5e)**. In parallel, in vitro angiogenesis assays showed robust enhancement of tube formation following treatment with (miR-OE) FUC-Exo, an effect that was effectively suppressed upon GW4869-mediated blockade of exosome release **(Figure 5f)**.

Collectively, these results indicate that ESCC cells actively deliver miR-6842-3p to endothelial cells via fucosylated exosomes, leading to increased endothelial permeability, augmented angiogenic activity, and facilitation of tumor progression.

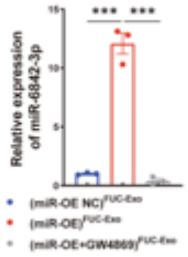
Relative expression of miR-6842-3p
(miR-OE NC)FUC-Exo
(miR-OE)FUC-Exo
(miR-OE+GW4869)FUC-Exo

a)

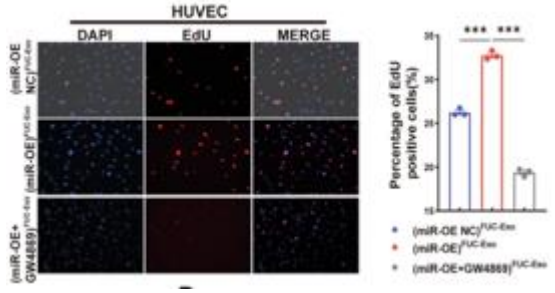
HUVEC
DAPI
EdU
MERGE
Percentage of EdU positive cells(%)

b)

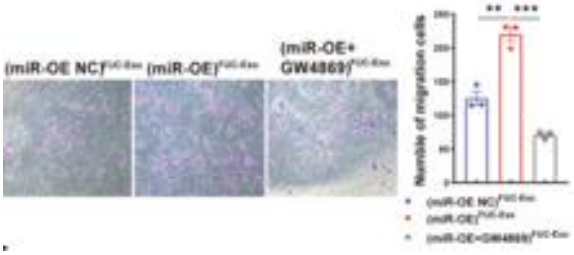
(miR-OE NC)FUC-Exo
(miR-OE)FUC-Exo
(miR-OE+GW4869)FUC-Exo
Number of migration cells

c)

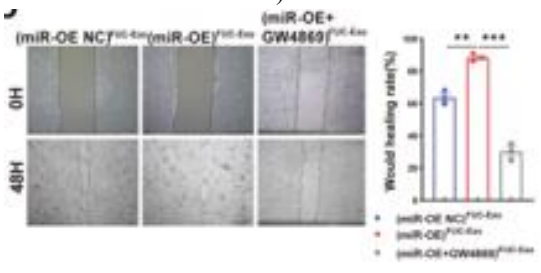
0H
48H
Would healing rate(%)

d)

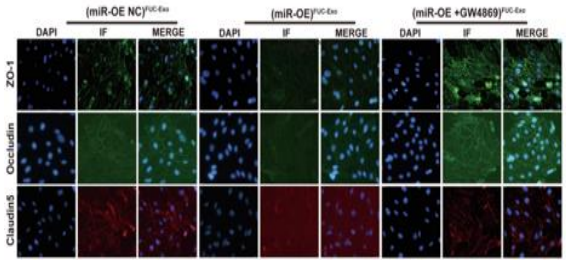
DAPI
IF
MERGE
ZO-1
Occludin
Claudin5

e)

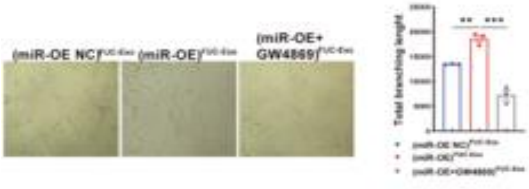
(miR-OE NC)FUC-Exo
(miR-OE)FUC-Exo
(miR-OE+GW4869)FUC-Exo
Total branching lenght

f)


xenografts
KYSE150 Cells (2×10⁶)
Subcutaneous injection
mouse xenografts
Observe 2 days
0 8 10 12 14 16 18 20 22 24 Days

g)

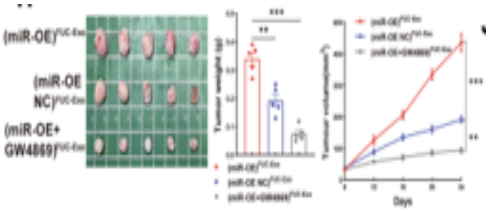
(miR-OE)FUC-Exo
(miR-OE NC)FUC-Exo
(miR-OE+GW4869)FUC-Exo
Tumor weight (g)
Tumor volume(mm³)
Days

h)

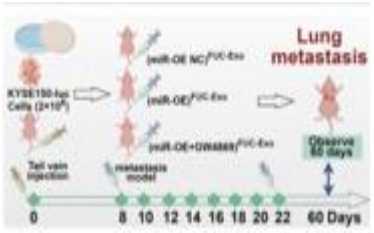
Lung metastasis
KYSE150-luc Cells (2×10⁶)
Tail vein injection
metastasis model
Observe 60 days
0 8 10 12 14 16 18 20 22 60 Days

j)

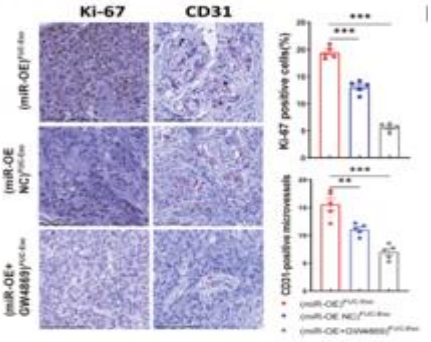
Ki-67
CD31
(miR-OE)FUC-Exo
(miR-OE NC)FUC-Exo
(miR-OE+GW4869)FUC-Exo
Ki-67 positive cells(%)
CD31 positive microvessels

i)

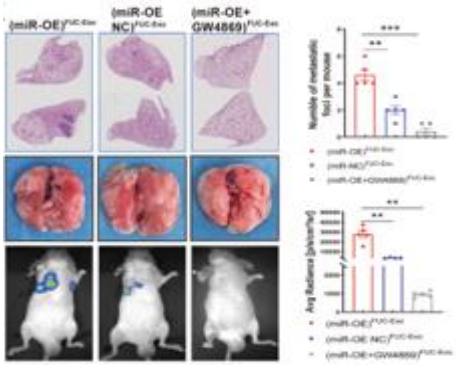

k)

Figure 5. Fucosylated exosomal miR-6842-3p enhances HUVEC proliferation, angiogenesis, and ESCC tumor progression.

(a) Levels of miR-6842-3p in HUVECs after treatment with various fucosylated exosome types—(miR-OE NC) FUC-Exo, (miR-OE) FUC-Exo, and (miR-OE + GW4869) FUC-Exo—were quantified using RT-qPCR (mean ± SEM, n = 3), ***p < 0.001. (b–d) Functional assays demonstrated the effect of these exosomes on HUVEC proliferation and migration: EDU incorporation (b), transwell migration (c), and wound closure (d) (scale bars, 100 μm); mean ± SEM, **p < 0.01, ***p < 0.001. (e) Immunofluorescence imaging revealed that treatment with FUC-Exo altered the expression of endothelial tight-junction proteins ZO-1, Occludin, and Claudin5 (scale bar, 50 μm). (f) Tube formation assays indicated that FUC-Exo exposure enhanced angiogenic capacity of HUVECs (scale bar, 100 μm); data are mean ± SEM, **p < 0.01, ***p < 0.001. (g) Schematic illustration of xenograft experimental design for testing FUC-Exo effects in vivo. (h) Representative xenograft images, tumour weight measurements, and growth curves of tumour volume demonstrate that (miR-OE) FUC-Exo accelerated tumour growth (mean ± SEM, n = 5). (i) IHC analysis for Ki-67 and CD31 in tumour sections shows increased proliferation and microvessel formation following (miR-OE) FUC-Exo treatment (scale bar, 100 μm; mean ± SEM, n = 5), **p < 0.01, ***p < 0.001. (j) Flowchart for assessment of lung metastasis in mice receiving FUC-Exo treatments. (K) H&E staining and representative images of lungs, along with IVIS quantification of fluorescent signal, demonstrate that (miR-OE) FUC-Exo promotes metastatic spread, whereas GW4869 reverses this effect (n = 5), **p < 0.01, ***p < 0.001.

To determine the in vivo role of fucosylated exosomal miR-6842-3p, xenograft and lung metastasis models were employed. In xenografts, KYSE150-derived tumours were treated every other day with 5 μg of the indicated fucosylated exosomes **(Figure 5g)**. Tumour measurements and immunohistochemistry for Ki-67 and CD31 revealed that (miR-OE) FUC-Exo significantly promoted tumour growth and angiogenesis, whereas these effects were blocked by GW4869 **(Figures 5h and 5i)**, confirming that fucosylated exosomes facilitate ESCC progression via miR-6842-3p transfer. For metastasis studies, 2 × 10^6 KYSE150-luc cells were injected into the tail vein of BALB/c nude mice. Starting eight days post-injection, mice received treatments with (miR-OE NC) FUC-Exo, (miR-OE) FUC-Exo, or (miR-OE + GW4869) FUC-Exo (5 μg) every other day, and lungs were harvested after two months **(Figure 5j)**. Analysis showed that (miR-OE) FUC-Exo enhanced lung metastatic burden, while GW4869 reduced it **(Figure 5k)**. These results indicate that fucosylated exosomes act as vehicles delivering miR-6842-3p to target cells, thereby driving tumour expansion, angiogenesis, and metastasis.

Fucosylated exosomal miR-6842-3p promotes angiogenesis via PTEN inhibition

To explore whether miR-6842-3p from fucosylated exosomes modulates angiogenesis through PTEN in endothelial cells, a dual-luciferase reporter assay confirmed a direct interaction between miR-6842-3p and PTEN in HUVECs. Fucosylated exosomes were then isolated from KYSE150 cells overexpressing miR-6842-3p and from TE-1 cells with miR-6842-3p knockdown. Exposure to these exosomes induced corresponding changes in PTEN mRNA levels in HUVECs. Furthermore, PTEN overexpression counteracted the miR-6842-3p-dependent effects on cell proliferation markers (PCNA, Cyclin D1), angiogenesis markers (MMP2, CD31), and tight junction proteins (Occludin, ZO-1, Claudin5) **(Figures 6a, 6e and 6f)**. Consistently, the ability of FUC-Exo to stimulate HUVEC proliferation, migration, and tube formation was abolished when PTEN was overexpressed **(Figures 6b–6d)**. These findings establish that fucosylated exosomal miR-6842-3p drives angiogenic activity in endothelial cells primarily by suppressing PTEN.

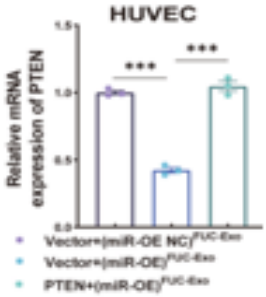

a)

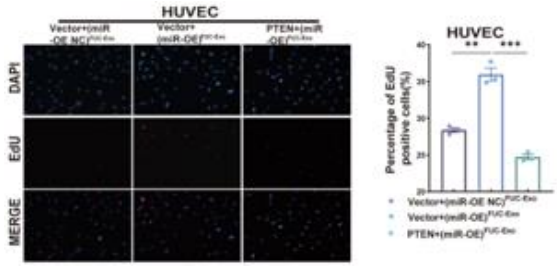

b)

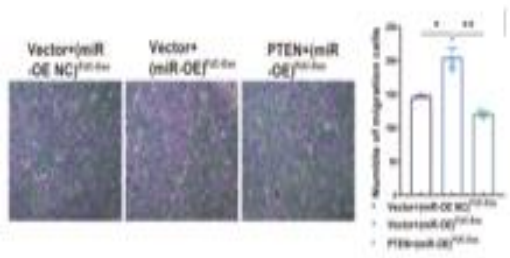

c)

d)

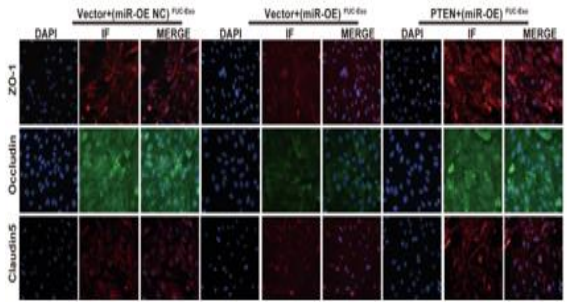

e)

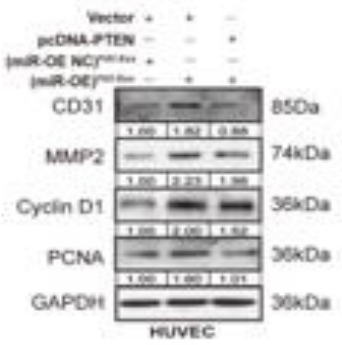

f)

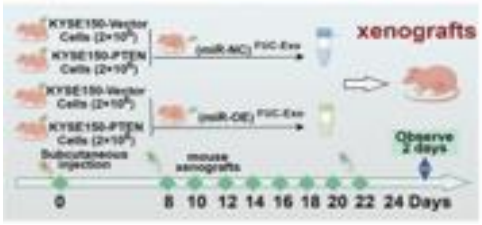

g)

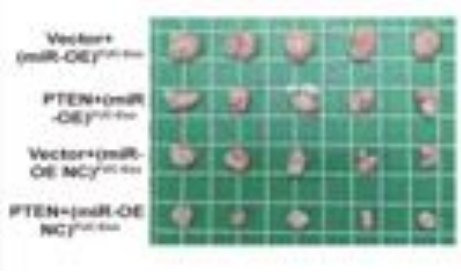

h)

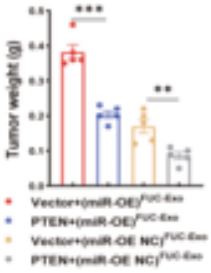

i)

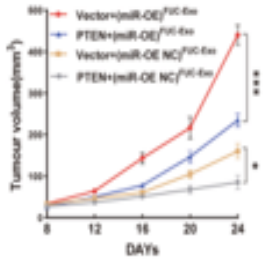

j)

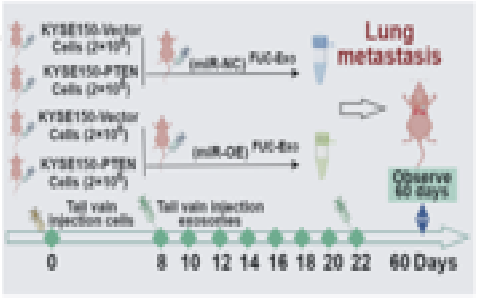

l)

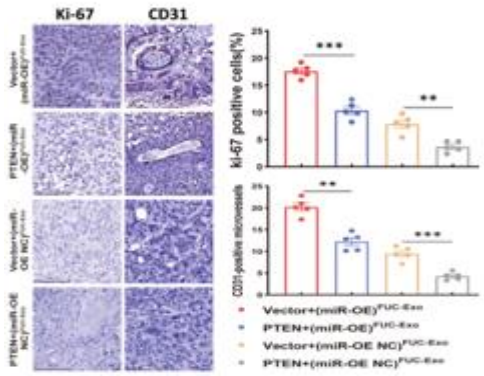

k)

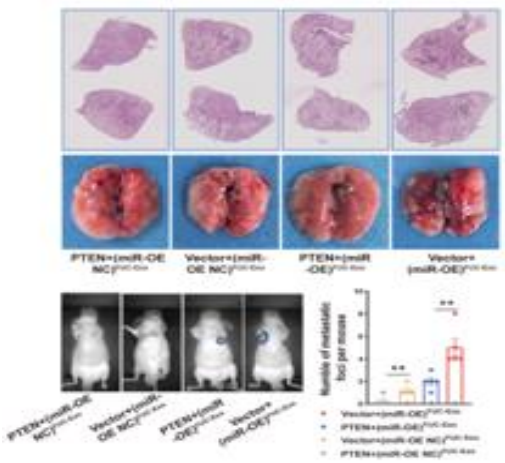

m)

Figure 6. Fucosylated exosome-derived miR-6842-3p enhances ESCC progression and angiogenesis via PTEN suppression.
(a) PTEN mRNA levels in HUVECs overexpressing PTEN (PTEN OE) after treatment with (miR-OE) FUC-Exo. Data are presented as mean ± SEM (n = 3), ***p < 0.001. (b–d) Assessment of PTEN overexpression on HUVEC proliferation (b), migration (c), and tube formation (d) following (miR-OE) FUC-Exo treatment. Scale bars, 100 μm. Data are shown as mean ± SEM (n = 3), *p < 0.05, **p < 0.01, ***p < 0.001. e Immunofluorescence analysis of tight junction proteins (ZO-1, Occludin, Claudin5) in HUVECs treated with (miR-OE) FUC-Exo and PTEN overexpression. Scale bar, 50 μm. f Western blot detection of proliferation markers (Cyclin D1, PCNA) and angiogenic markers (MMP2, CD31) in HUVECs under indicated treatments. Protein levels normalized to GAPDH were quantified. g Schematic outlining the xenograft model experimental workflow for evaluating tumor proliferation. H–K Representative xenograft tumor images (h), tumor weights (i), tumor growth curves (j), and IHC analysis of Ki-67 and CD31 in tumors (k). Scale bar, 100 μm. Data shown as mean ± SEM (n = 5), **p < 0.01, ***p < 0.001. l Diagram of experimental setup for lung metastasis evaluation. m Representative lung images and H&E staining (scale bar, 1 μm), quantification of metastatic nodules, and total fluorescent intensity in lungs. Data presented as mean ± SEM (n = 5), **p < 0.01, ***p < 0.001.

To validate the role of fucosylated exosomal miR-6842-3p in ESCC progression, we employed xenograft models, lung metastasis assays, and in vivo Matrigel plug angiogenesis experiments **(Figures 6g–6m)**. As illustrated in **Figures 6h–6k**, treatment with (miR-OE) FUC-Exo significantly enhanced ESCC tumor growth, metastasis, and angiogenesis, effects that were notably reversed by PTEN overexpression. IHC staining confirmed elevated Ki-67 and CD31 levels in tumors from the (miR-OE) FUC-Exo group, whereas PTEN overexpression blocked this induction **(Figure 6k)**. Similarly, in the Matrigel plug assay, miR-OE exosome-treated plugs exhibited extensive vascularization, which was negated by PTEN overexpression. Collectively, these results indicate that ESCC-derived fucosylated exosomal miR-6842-3p promotes tumor angiogenesis and progression through PTEN inhibition in vivo.

Fucosylated exosomal miR-6842-3p drives ESCC angiogenesis through AKT/mTOR pathway activation
PTEN, a canonical tumor suppressor, governs multiple cellular processes including proliferation and differentiation, largely via its phosphatase-mediated modulation of signaling pathways such as AKT/mTOR [19]. To elucidate the mechanism by which fucosylated exosomal miR-6842-3p facilitates ESCC progression and angiogenesis, transcriptome sequencing followed by KEGG enrichment analysis was conducted. Genes downregulated by miR-6842-3p were significantly enriched in eight pathways, including PI3K/AKT and chemokine signaling pathways, which were prioritized for further analysis due to their critical roles in tumor angiogenesis and progression [20] **(Figure 7a)**.
Subsequently, fucosylated exosomes were isolated from KYSE150 and TE-1 ESCC cells with stable miR-6842-3p overexpression or knockdown and used to treat HUVECs. Western blot results demonstrated that (miR-OE) FUC-Exo reduced PTEN protein levels while

increasing p-AKT and p-mTOR expression. Conversely, (miR-KD) FUC-Exo elevated PTEN and decreased p-AKT/p-mTOR levels **(Figure 7b)**. Rescue assays showed that PTEN overexpression partially reversed (miR-OE) FUC-Exo-mediated p-AKT and p-mTOR activation **(Figure 7c)**. Furthermore, the AKT inhibitor Ipatasertib abolished (miR-OE) FUC-Exo-induced p-mTOR upregulation in HUVECs **(Figure 7d)**. Functional studies confirmed that the proliferative, migratory, and angiogenic effects induced by (miR-OE) FUC-Exo were blocked by either Ipatasertib or Rapamycin **(Figures 7e–7j)**.

Overall, these findings reveal that fucosylated exosomal miR-6842-3p promotes angiogenesis in ESCC by suppressing PTEN expression and activating the AKT/mTOR signaling axis.

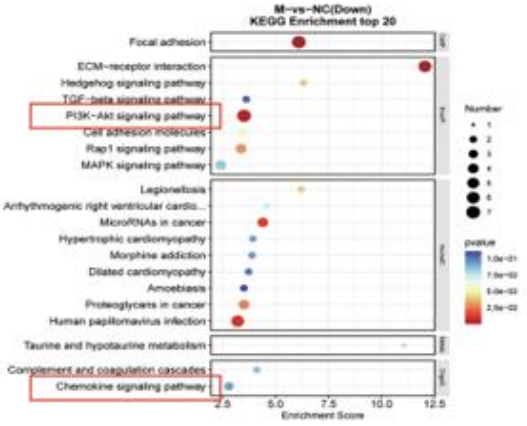

a)

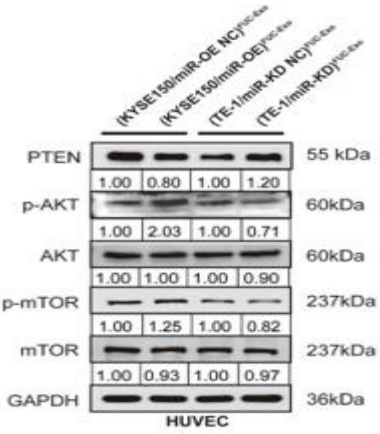

b)

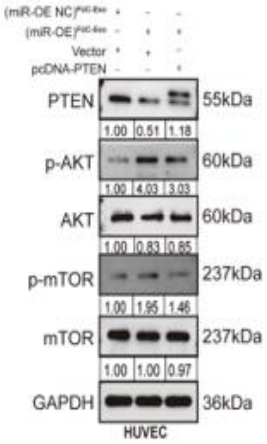

c)

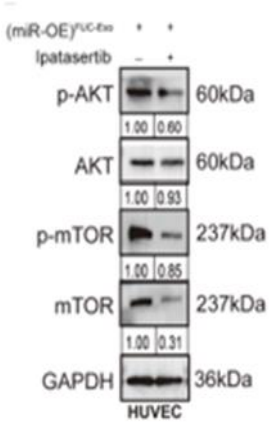

d)

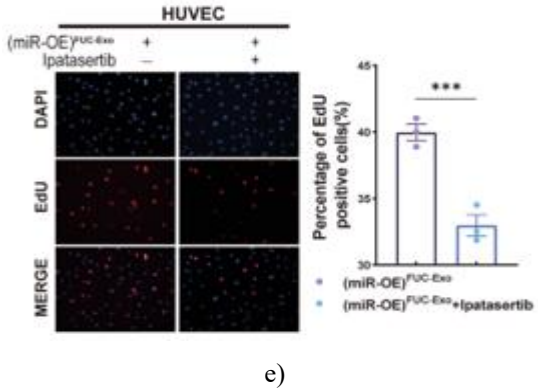

e)

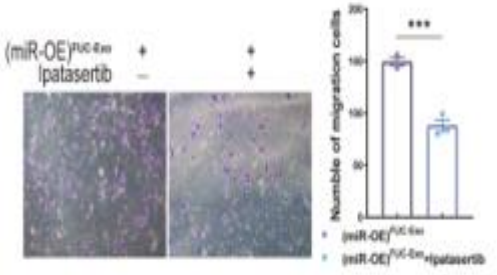

f)

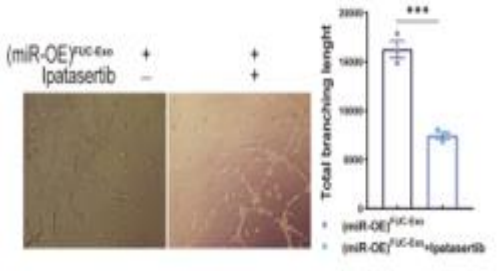

g)

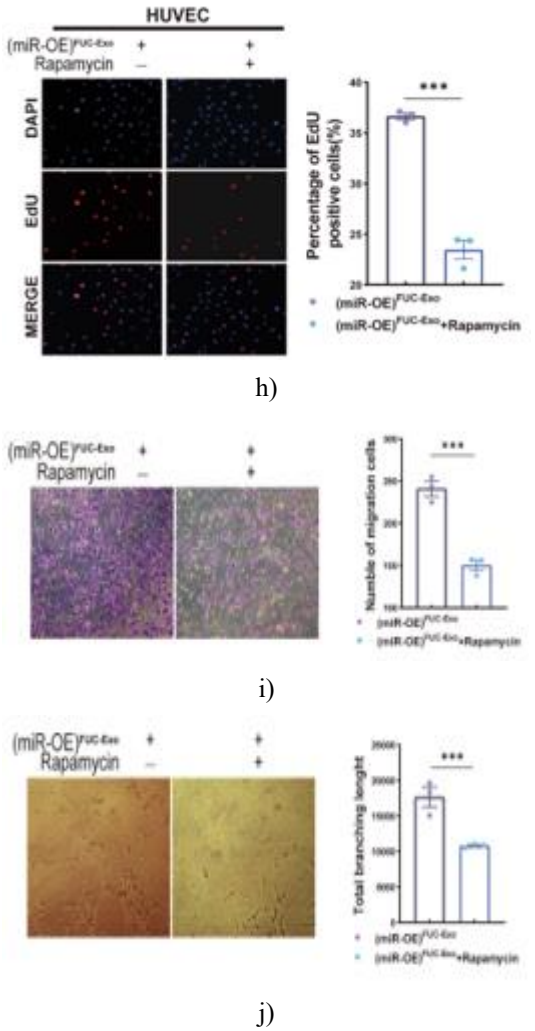

Figure 7. Fucosylated exosomal miR-6842-3p drives esophageal squamous cell carcinoma (ESCC) angiogenesis by activating the AKT/mTOR signaling pathway.

(a) Results from KEGG pathway enrichment analysis of differentially expressed genes (DEGs), with bar charts emphasizing the PI3K/AKT and chemokine signaling pathways.

(b) Western blot showing protein expression levels of PTEN, total AKT, phosphorylated AKT (p-AKT), total mTOR, and phosphorylated mTOR (p-mTOR) in human umbilical vein endothelial cells (HUVECs) exposed to the specified fucosylated exosomes.

(c) Western blot detection of key proteins in the PTEN/AKT/mTOR signaling cascade under the various treatment conditions indicated.

(d) Western blot evaluation of AKT/mTOR pathway proteins in HUVECs treated with miR-6842-3p-overexpressing (miR-OE) fucosylated exosomes, with or without the AKT inhibitor Ipatasertib.

(e–g) Impact of the AKT inhibitor Ipatasertib on cell proliferation, migration, and tube formation in HUVECs treated with (miR-OE) fucosylated exosomes, as assessed by EdU incorporation assay (scale bar, 100 μm) (e), transwell migration assay (scale bar, 100 μm) (f), and in vitro tube formation assay (scale bar, 100 μm) (g).

(h–i) Influence of the mTOR inhibitor Rapamycin on proliferation, migration, and angiogenic capacity of (miR-OE) fucosylated exosome-treated HUVECs, determined using EdU assay (scale bar, 100 μm) (h), migration assay (scale bar, 100 μm) (i), and tube formation assay (scale bar, 100 μm) (j).

Results are expressed as mean ± SEM from at least three independent experiments; **p < 0.01, ***p < 0.001. Note: Protein bands were quantified by densitometry relative to GAPDH loading control.

Fucosylated exosomal miR-6842-3p enhances ESCC angiogenesis through suppression of CXCL10 via the AKT/mTOR signaling pathway

Cytokines present in the tumor microenvironment (TME) are essential for driving tumor progression and new blood vessel formation. Pathway enrichment analysis demonstrated involvement of the chemokine signaling axis in the tumor-promoting actions of fucosylated exosomal miR-6842-3p **(Figure 7a)**. To delve deeper, HUVECs were exposed to either (miR-OE) or control (miR-OE NC) fucosylated exosomes, followed by assessment of cytokine expression using a human cytokine antibody array. Treatment with fucosylated exosomes led to a notable downregulation of CXCL10 (also referred to as IP-10) **(Figure 8a)**. CXCL10 is established as a potent inhibitor of angiogenesis, mediating its effects via CXCR3-dependent and -independent routes, such as restraining endothelial cell proliferation, migration, and viability while triggering apoptosis [21–23]. The tumor-suppressive and anti-angiogenic functions of CXCL10 are well-documented across numerous malignancies [24–26]. As one example, miR-21-5p has been shown to reduce CXCL10 levels, thereby facilitating angiogenesis in ESCC [4]. Based on these data, we postulate that CXCL10 functions as a key downstream mediator of the AKT/mTOR pathway controlled by fucosylated exosomal miR-6842-3p.

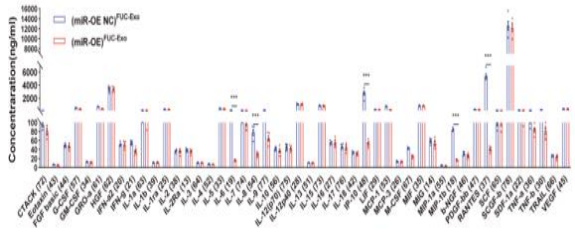

a)

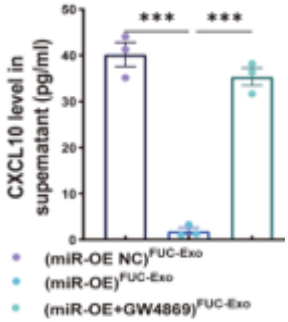

b)

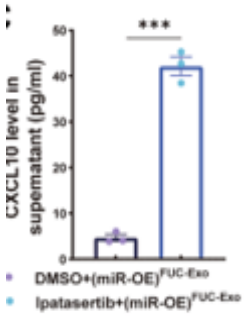

c)

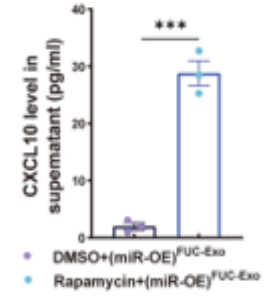

d)

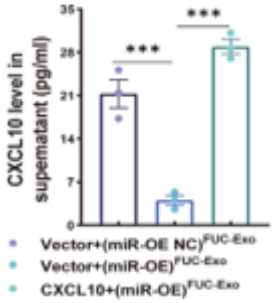

e)

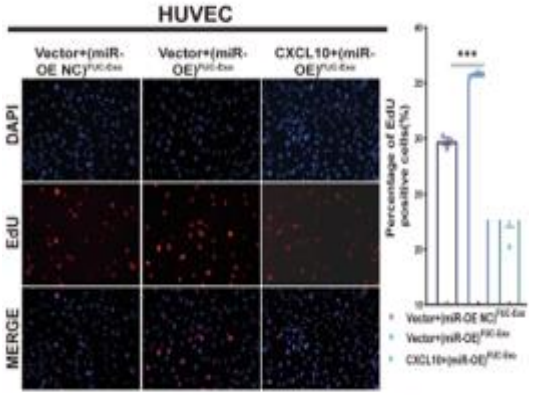

f)

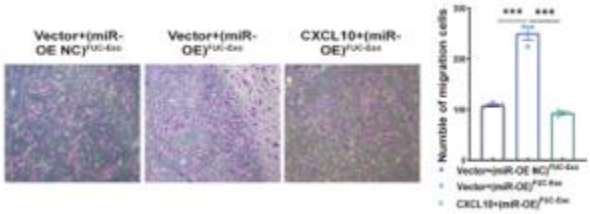

g)

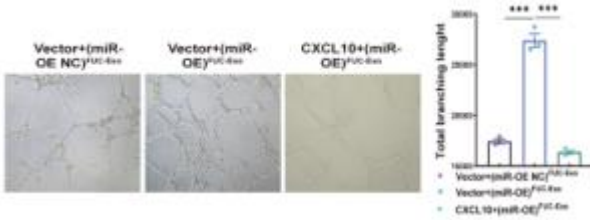

h)

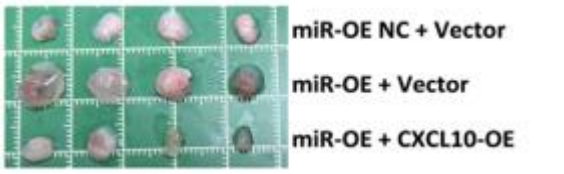

i)

j)

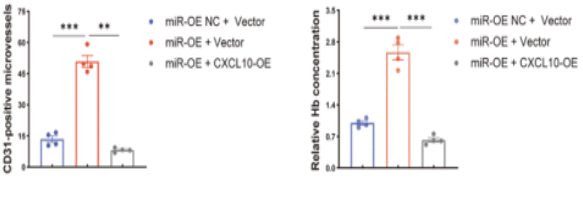

k)

Figure 8. Fucosylated exosomal miR-6842-3p facilitates angiogenesis in esophageal squamous cell carcinoma (ESCC) by suppressing CXCL10 through the AKT/mTOR pathway.

(a) Cytokine profiling in culture media from HUVECs exposed to (miR-OE) or (miR-OE NC) fucosylated exosomes, performed using a human cytokine antibody array. Values shown as mean ± SEM (n = 3), **p < 0.01, ***p < 0.001.

(b) Secreted CXCL10 concentrations measured by ELISA in HUVECs after treatment with (miR-OE

NC) fucosylated exosomes, (miR-OE) fucosylated exosomes, or (miR-OE + GW4869) fucosylated exosomes. Values shown as mean ± SEM (n = 3), ***p < 0.001.

(c–d) ELISA quantification of extracellular CXCL10 in (miR-OE) fucosylated exosome-treated HUVECs co-treated with either the AKT blocker Ipatasertib (c) or the mTOR blocker Rapamycin (d). Values shown as mean ± SEM (n = 3), ***p < 0.001.

(e) ELISA detection of CXCL10 in media from (miR-OE) fucosylated exosome-treated HUVECs following forced CXCL10 overexpression. Values shown as mean ± SEM (n = 3), ***p < 0.001.

(f–h) Consequences of CXCL10 overexpression on endothelial proliferation, migration, and vessel-forming ability in (miR-OE) fucosylated exosome-exposed HUVECs, assessed via EdU proliferation assay (scale bar, 100 μm) (f), migration assay (scale bar, 100 μm) (g), and tube formation assay (scale bar, 100 μm) (h). Values shown as mean ± SEM (n = 3), *p < 0.05, ***p < 0.001.

(i–k) Images of harvested Matrigel plugs containing HUVECs transduced with miR-OE NC + Vector, miR-OE + Vector, or miR-OE + CXCL10-OE (i). CD31 immunohistochemistry highlighting microvascular structures within plugs (j). Hemoglobin content as an indicator of plug vascularization (k). **p < 0.01, ***p < 0.001, n = 4 per group.

Additional ELISA data confirmed that exposure to (miR-OE) fucosylated exosomes strongly curtailed CXCL10 release from HUVECs compared with control conditions **(Figure 8b)**, whereas inhibiting exosome release with GW4869 in the miR-OE context restored CXCL10 secretion **(Figure 8b)**. Blocking either AKT with Ipatasertib or mTOR with Rapamycin prevented the CXCL10 suppression triggered by (miR-OE) fucosylated exosomes **(Figures 8c and 8d)**. Forced CXCL10 expression largely overcame the inhibitory effect of (miR-OE) fucosylated exosomes on CXCL10 levels **(Figure 8e)**. In functional assays, elevating CXCL10 markedly blunted the stimulation of proliferation, migration, and tube formation conferred by (miR-OE) fucosylated exosomes **(Figures 8f–8h)**. Consistent with in vitro findings, in vivo Matrigel plug experiments revealed that CXCL10 overexpression effectively counteracted the enhanced vascularization driven by miR-6842-3p **(Figures 8i–8k)**. Altogether, these results substantiate that fucosylated exosomal miR-6842-3p stimulates ESCC-associated angiogenesis primarily by repressing CXCL10 via AKT/mTOR activation.

Fucosylated exosomal miR-6842-3p restricts CXCL10 secretion by impairing IRF1 expression through AKT/mTOR pathway engagement

To uncover how heightened fucosylated exosomal miR-6842-3p curbs CXCL10 levels, we turned to prior reports. In hepatocellular carcinoma models, IRF1 transcript abundance correlates positively with CXCL10, and IRF1-binding motifs have been mapped in the CXCL10 promoter region [27]. Furthermore, chromatin immunoprecipitation coupled with qPCR has validated that IRF1 occupancy drives CXCL10 gene activation, thereby bolstering antitumor immune activity [27]. Separate work has revealed that interfering with PI3K/AKT/mTOR signaling elevates CXCL10 and CXCL11 production by increasing IRF1 [28]. Guided by this evidence, we posited that fucosylated exosomal miR-6842-3p limits CXCL10 output by diminishing IRF1—a crucial transcription factor for CXCL10—via AKT/mTOR pathway involvement.

Western blotting initially disclosed that IRF1 protein abundance dropped sharply in HUVECs receiving (miR-OE) fucosylated exosomes, while it rose after (miR-KD) fucosylated exosome treatment relative to controls, verifying IRF1 downregulation by the miR-overexpressing exosomes **(Figure 9a)**. Given reports that PI3K/AKT/mTOR blockade raises CXCL10/CXCL11 through IRF1 [28], we tested if this cascade governs IRF1 in the context of fucosylated exosomal miR-6842-3p. Overexpressing PTEN partly counteracted the IRF1 reduction imposed by (miR-OE) fucosylated exosomes **(Figure 9b)**. Similarly, applying Ipatasertib or Rapamycin neutralized the IRF1 decline elicited by (miR-OE) fucosylated exosomes **(Figures 9c and 9d)**. In summary, these observations reveal that fucosylated exosomal miR-6842-3p lowers IRF1 levels by activating the AKT/mTOR axis.

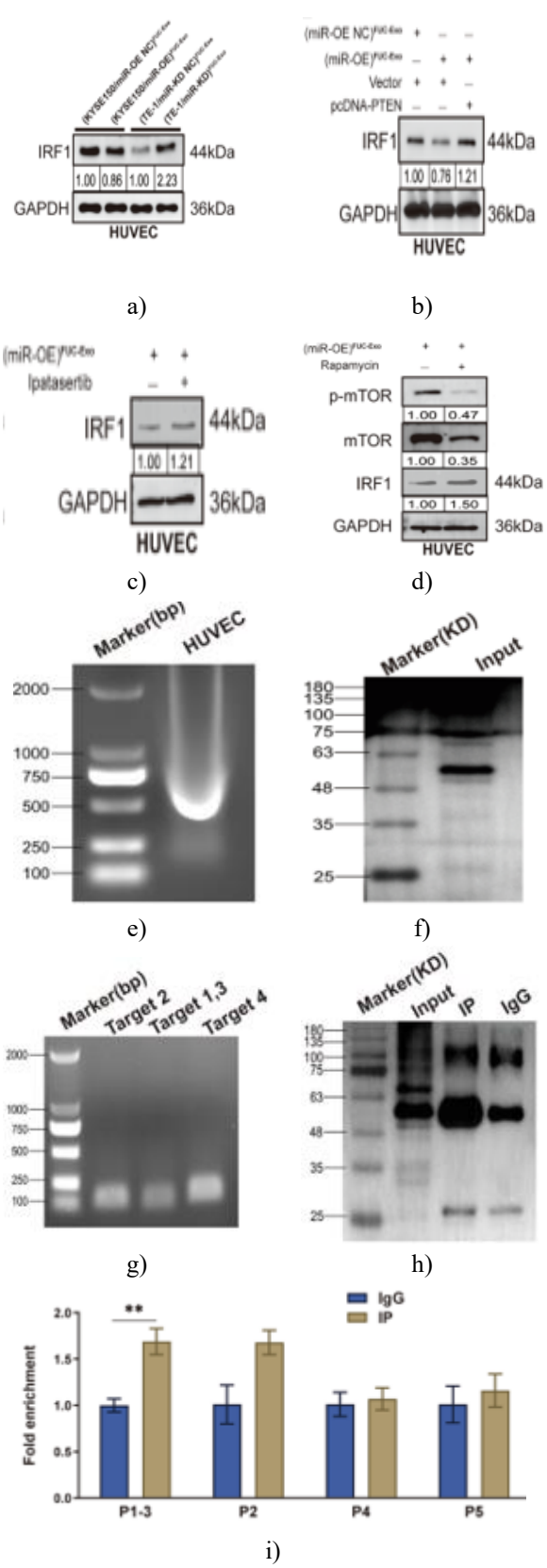

Figure 9. Fucosylated exosomal miR-6842-3p restricts CXCL10 secretion by reducing IRF1 expression through the AKT/mTOR signaling pathway.

(a) Western blot evaluation of IRF1 protein levels in HUVECs exposed to the specified fucosylated exosomes.

(b) Western blot assessment of IRF1 expression in HUVECs subjected to the indicated experimental conditions.

(c) Western blot detection of IRF1 in HUVECs treated with (miR-OE) fucosylated exosomes, with or without the AKT inhibitor Ipatasertib.

(d) Western blot analysis of mTOR, phosphorylated mTOR (p-mTOR), and IRF1 levels in (miR-OE) fucosylated exosome-treated HUVECs, in the presence or absence of the mTOR inhibitor Rapamycin.

(e–j) Evidence that IRF1 drives CXCL10 transcription.

(e) Agarose gel image demonstrating chromatin fragmentation efficiency after sonication. Left lane: D2000 DNA marker (bands at 2000 bp, 1000 bp, 750 bp, 500 bp, 250 bp, 100 bp); Right lane: Sheared chromatin DNA from HUVECs.

(f) Western blot of the input nuclear extract from HUVECs, showing a distinct IRF1 band at approximately 50 kDa, confirming protein presence.

(g) Agarose gel electrophoresis of ChIP-PCR amplicons from various target regions.

(h) Western blot confirming IRF1 enrichment in immunoprecipitated samples.

(i) Quantitative ChIP-qPCR results showing IRF1 binding enrichment. Data are mean ± SD, **p < 0.01.

(j) Diagram illustrating predicted IRF1-binding motifs in the human CXCL10 promoter, identified through bioinformatics prediction.

Since IRF1 serves as a key transcriptional activator of CXCL10, we explored its direct role in promoting CXCL10 expression. Consistent with published data [27], mining of The Cancer Genome Atlas (TCGA) dataset indicated a strong positive association between IRF1 and CXCL10 mRNA levels in ESCC samples. To uncover the underlying mechanism, we used computational tools to identify five candidate IRF1-binding sites within the human CXCL10 promoter. Subsequent chromatin immunoprecipitation followed by quantitative PCR (ChIP-qPCR) confirmed IRF1 occupancy, with the most robust enrichment observed at Targets 1–3—particularly in conserved regions—when using an anti-IRF1 antibody compared to IgG controls **(Figures 9e–9j)**. Overall, these experiments establish that IRF1 directly binds the CXCL10 promoter to enhance its transcription in endothelial cells. Integrating these observations with earlier findings, we conclude that fucosylated exosomal miR-6842-3p inhibits CXCL10 production by suppressing IRF1 expression via AKT/mTOR pathway activation.

This study presents robust evidence establishing fucosylated exosomal miR-6842-3p as a central driver of angiogenesis in esophageal squamous cell carcinoma (ESCC) through the PTEN/AKT/mTOR/IRF1/CXCL10 signaling cascade. We demonstrate that miR-6842-3p, packaged in fucosylated exosomes released by ESCC cells, is delivered to endothelial cells, where it represses PTEN, leading to heightened AKT/mTOR activity, reduced IRF1 levels, and consequent downregulation of the anti-angiogenic factor CXCL10. This sequence of events accelerates endothelial proliferation, migration, tube formation, tumor vascularization, growth, and metastatic spread in preclinical models. Beyond delineating a previously unrecognized pathway by which tumor-derived fucosylated exosomes reshape the tumor microenvironment, our work positions miR-6842-3p as a promising candidate for ESCC diagnosis and prognostication.

Emerging research has highlighted exosomal microRNAs as vital conduits for crosstalk in cancer, especially in ESCC, facilitating remodeling of the surrounding stroma [29, 30]. Our investigation extends these insights by pinpointing miR-6842-3p as markedly enriched in fucosylated exosomes from ESCC patient sera. Its detectable elevation even in early disease stages points to utility as a minimally invasive tool for screening. Indeed, serum fucosylated exosomal miR-6842-3p outperformed traditional markers such as SCC-Ag and CEA in diagnostic accuracy **(Figure 1b)**. Furthermore, higher circulating levels strongly associated with aggressive disease features and unfavorable survival outcomes, reinforcing its prognostic value **(Figures 1c–1f)**. These observations resonate with growing evidence supporting exosomal miRNAs as reliable liquid biopsy markers across malignancies [31, 32].

Dysregulated microRNA (miRNA) expression plays a central role in the initiation and advancement of many human malignancies [33, 34]. To date, however, the functional contributions of miR-6842-3p to cancer biology remain unexplored. In this work, we show that miR-6842-3p is markedly enriched in serum fucosylated exosomes (FUC-Exo) while remaining unaltered in unfractionated serum exosomes [11]. This selective enrichment arises from two primary processes:

1. Targeted incorporation into FUC-Exo elevates miR-6842-3p levels. Exosomal cargo loading is governed by specialized, cell-specific mechanisms, such as miRNA interactions with RNA-binding proteins (RBPs) or associations with endosomal lipid rafts [35]. Paralleling our earlier observation that the tumor-suppressive miR-4732-3p is preferentially loaded into FUC-Exo via hnRNPK to prevent inhibition of lung cancer growth [7, 36], miR-6842-3p appears to undergo similar selective packaging. Consistent with this, forced expression of miR-6842-3p in ESCC cells dramatically boosted its abundance in released FUC-Exo **(Figures 4c and 4d)**; strikingly, although intracellular levels rose by tens to hundreds of fold in stably modified ESCC cells, extracellular enrichment in FUC-Exo reached thousands of fold **(Figures 4c and 4d)**. These patterns indicate that ESCC-derived FUC-Exo harbor dedicated machinery for concentrating miR-6842-3p.
2. A dilution effect in bulk exosomes conceals the increase in miR-6842-3p. Unfractionated serum exosomes comprise a diverse pool, including (i) non-fucosylated exosomes (lacking preferential miR-6842-3p loading) and (ii) exosomes secreted by normal cells (which produce little miR-6842-3p). Since FUC-Exo represent only a fraction of total exosomes, the heightened miR-6842-3p within them is masked by these low-expressing subpopulations, yielding no overall change in bulk serum exosome levels despite clear upregulation in the FUC-Exo subset.

To assess the functional impact of this FUC-Exo-enriched miR-6842-3p in ESCC, we performed comprehensive in vitro and in vivo assays. These revealed that miR-6842-3p drives ESCC cell proliferation, migration, invasion, and epithelial-mesenchymal transition (EMT), establishing its pro-oncogenic activity. Although tumor-released exosomes frequently shuttle miRNAs to repress target genes in recipient cells [37, 38], the specific involvement of fucosylated exosomal miRNAs in ESCC advancement has been understudied. Our mechanistic studies showed that miR-6842-3p exerts these effects by directly suppressing PTEN, a classic tumor suppressor that restrains the PI3K/AKT/mTOR cascade [39, 40]. PTEN loss is common in ESCC and linked to disease progression and unfavorable outcomes [41]. In agreement, miR-6842-3p-driven PTEN inhibition activated AKT signaling in ESCC cells, fueling tumor advancement. These observations parallel reports of exosomal miRNAs targeting PTEN in ovarian and liver cancers [42, 43]. Notably, our work pioneers the connection between fucosylated exosome-delivered miR-6842-3p and PTEN control in ESCC.

Fucosylation, a key glycosylation modification, increasingly influences cancer pathogenesis by affecting exosome formation and activity [6, 7]. Building on our previous evidence that fucosylated exosomes predominate among tumor-derived vesicles and accelerate malignancy [7, 36], we here establish that miR-6842-3p is preferentially loaded into these exosomes and shuttled to endothelial cells. There, it represses CXCL10—a potent anti-angiogenic factor—promoting vascularization. CXCL10 curbs endothelial proliferation, migration, and survival; its downregulation by miR-6842-3p thus fosters the angiogenic switch in ESCC **(Figure 8)**, mirroring its established anti-vascular roles across tumors [21–23].

The AKT/mTOR axis potently governs angiogenesis and stromal remodeling [44], with hyperactivation tied to progression in diverse cancers [19, 20]. IRF1 transcriptionally drives CXCL10 expression [45], and CXCL10 limits neovascularization in settings like corneal injury and tumors such as Kaposi sarcoma [24–26, 46]. We uncovered that miR-6842-3p, via PTEN suppression, engages AKT/mTOR to diminish IRF1 and subsequently CXCL10 **(Figures 8 and 9)**. This aligns with evidence that blocking PI3K/AKT/mTOR restores CXCL10 through IRF1 upregulation [28], positioning the miR-6842-3p/PTEN/AKT/mTOR/IRF1/CXCL10 cascade as a prime interventional node for ESCC vascularization.

Despite these advances, limitations persist. Independent large-scale cohorts are required to confirm fucosylated exosomal miR-6842-3p as a robust prognostic tool. Xenografts imperfectly mimic human ESCC; patient-derived xenografts would strengthen translational relevance. While PTEN is a validated direct target, additional miR-6842-3p effectors likely exist and merit investigation. Although we demonstrated in vivo metastatic promotion by fucosylated exosomal miR-6842-3p, real-time tracking (e.g., via fluorescent labeling) of exosome biodistribution is needed. Critically, two unresolved issues loom: the precise machinery directing miR-6842-3p into FUC-Exo, and standardized protocols for isolating and characterizing FUC-Exo. Addressing these will advance exosome biogenesis knowledge and miRNA packaging in ESCC.

Conclusion

Overall, this investigation establishes that fucosylated exosomal miR-6842-3p fuels ESCC angiogenesis through the PTEN/AKT/mTOR/IRF1/CXCL10 pathway. These insights expand our grasp of ESCC angiogenic drivers and nominate miR-6842-3p as an attractive biomarker and therapeutic prospect for the disease.

Acknowledgments: None

Conflict of Interest: None

Financial Support: None

Ethics Statement: None

References

1. Guo D, Jin J, Li D, He Y, Lin Y. Analysis of the incidence and mortality trends of esophageal cancer in cancer registry areas of China and Japan. Int J Cancer. 2024;155:1376–1386.
2. Sheikh M, Roshandel G, McCormack V, Malekzadeh R. Current status and future prospects for esophageal cancer. Cancers. 2023;15:765.
3. Yin X, Tian M, Zhang J, Tang W, Feng L, Li Z, et al. MiR-26b-5p in small extracellular vesicles derived from dying tumor cells after irradiation

enhances the metastasis promoting microenvironment in esophageal squamous cell carcinoma. Cancer Lett. 2022;541:215746.
4. Zhang Y, Chen C, Liu Z, Guo H, Lu W, Hu W, et al. PABPC1-induced stabilization of IFI27 mRNA promotes angiogenesis and malignant progression in esophageal squamous cell carcinoma through exosomal miRNA-21-5p. J Exp Clin Cancer Res. 2022;41:111.
5. Xiao Z, Zhao J, Ji G, Song X, Xue X, Zhang W, et al. miR-493-5p silenced by DNA methylation promotes angiogenesis via exosomes and VEGF-a-mediated intracellular cross-talk between ESCC cells and HUVECs. Int J Nanomed. 2024;19:7165–7183.
6. Jia L, Zhang J, Ma T, Guo Y, Yu Y, Cui J. The function of fucosylation in progression of lung cancer. Front Oncol. 2018;8:565.
7. Zhuang W, Liu C, Hong Y, Zheng Y, Huang M, Tang H, et al. Tumor-suppressive miR-4732-3p is sorted into fucosylated exosome by hnRNPK to avoid the inhibition of lung cancer progression. J Exp Clin Cancer Res. 2024;43:123.
8. Théry C, Witwer KW, Aikawa E, Alcaraz MJ, Anderson JD, Andriantsitohaina R, et al. Minimal information for studies of extracellular vesicles 2018 (MISEV2018): a position statement of the International Society for Extracellular Vesicles and update of the MISEV2014 guidelines. J Extracell Vesicles. 2018;7:1535750.
9. Ohtsubo K, Marth JD. Glycosylation in cellular mechanisms of health and disease. Cell. 2006;126:855–867.
10. Vrablova V, Kosutova N, Blsakova A, Bertokova A, Kasak P, Bertok T, et al. Glycosylation in extracellular vesicles: isolation, characterization, composition, analysis and clinical applications. Biotechnol Adv. 2023;67:108196.
11. Chen J, Zheng Y, Wang Z, Gao Q, Hao K, Chen X, et al. Development a glycosylated extracellular vesicle-derived miRNA Signature for early detection of esophageal squamous cell carcinoma. BMC Med. 2025;23:39.
12. Mu X, Yu C, Zhao Y, Hu X, Wang H, He Y, et al. Exosomal miR-1228-5p down-regulates DUSP22 to promotes cell proliferation and migration in small cell lung cancer. Life Sci. 2024;351:122787.
13. Gramantieri L, Pollutri D, Gagliardi M, Giovannini C, Quarta S, Ferracin M, et al. MiR-30e-3p influences tumor phenotype through MDM2/TP53 axis and predicts sorafenib resistance in hepatocellular carcinoma. Cancer Res. 2020;80:1720–1734.
14. Cao J, Shao H, Hu J, Jin R, Feng A, Zhang B, et al. Identification of invasion-metastasis associated MiRNAs in gallbladder cancer by bioinformatics and experimental validation. J Transl Med. 2022;20:188.
15. Zhang X, Kschischo M. Distinct and common features of numerical and structural chromosomal instability across different cancer types. Cancers. 2022;14:1424.
16. Carnero A, Blanco-Aparicio C, Renner O, Link W, Leal JF. The PTEN/PI3K/AKT signalling pathway in cancer, therapeutic implications. Curr cancer drug targets. 2008;8:187–198.
17. Li L, Ross AH. Why is PTEN an important tumor suppressor?. J Cell Biochem. 2007;102:1368–1374.
18. Kulkarni B, Kirave P, Gondaliya P, Jash K, Jain A, Tekade RK, et al. Exosomal miRNA in chemoresistance, immune evasion, metastasis and progression of cancer. Drug Discov Today. 2019;24:2058–2067.
19. He YM, Zhou XM, Jiang SY, Zhang ZB, Cao BY, Liu JB, et al. TRIM25 activates AKT/mTOR by inhibiting PTEN via K63-linked polyubiquitination in non-small cell lung cancer. Acta Pharmacol Sin. 2022;43:681–691.
20. Vara Fresno, Casado JA, de Castro E, Cejas J, Belda-Iniesta P, González-Barón C. M: PI3K/Akt signalling pathway and cancer. Cancer Treat Rev. 2004;30:193–204.
21. Liu M, Guo S, Stiles JK. The emerging role of CXCL10 in cancer (review). Oncol Lett. 2011;2:583–589.
22. Billottet C, Quemener C, Bikfalvi A. CXCR3, a double-edged sword in tumor progression and angiogenesis. Biochim Biophys Acta. 2013;1836:287–295. CAS PubMed Google Scholar
23. Zhou C, Gao Y, Ding P, Wu T, Ji G. The role of CXCL family members in different diseases. Cell Death Discov. 2023;9:212.
24. Gao N, Liu X, Wu J, Li J, Dong C, Wu X, et al. CXCL10 suppression of hem- and lymph-angiogenesis in inflamed corneas through MMP13. Angiogenesis. 2017;20:505–518.
25. Dinsart C, Pervolaraki K, Stroh-Dege A, Lavie M, Ronsse I, Rommelaere J, et al. Recombinant

parvoviruses armed to deliver CXCL4L1 and CXCL10 are impaired in their antiangiogenic and antitumoral effects in a Kaposi sarcoma tumor model due to the chemokines' interference with the virus cycle. Hum Gene Ther. 2017;28:295–306.
26. Ishiuchi Y, Sato H, Tsujimura K, Kawaguchi H, Matsuwaki T, Yamanouchi K, et al. Skeletal muscle cell contraction reduces a novel myokine, chemokine (C-X-C motif) ligand 10 (CXCL10): potential roles in exercise-regulated angiogenesis. Biosci Biotechnol Biochem. 2018;82:97–105.
27. Yan Y, Zheng L, Du Q, Yazdani H, Dong K, Guo Y, et al. Interferon regulatory factor 1(IRF-1) activates anti-tumor immunity via CXCL10/CXCR3 axis in hepatocellular carcinoma (HCC). Cancer Lett. 2021;506:95–106.
28. Kumagai S, Togashi Y, Sakai C, Kawazoe A, Kawazu M, Ueno T, et al. An oncogenic alteration creates a microenvironment that promotes tumor progression by conferring a metabolic advantage to regulatory T cells. Immunity. 2020;53:187–203.e188.
29. Xue ST, Zheng B, Cao SQ, Ding JC, Hu GS, Liu W, et al. Long non-coding RNA LINC00680 functions as a ceRNA to promote esophageal squamous cell carcinoma progression through the miR-423-5p/PAK6 axis. Mol Cancer. 2022;21:69.
30. Li K, Lin Y, Luo Y, Xiong X, Wang L, Durante K, et al. A signature of saliva-derived exosomal small RNAs as predicting biomarker for esophageal carcinoma: a multicenter prospective study. Mol Cancer. 2022;21:21.
31. Preethi KA, Selvakumar SC, Ross K, Jayaraman S, Tusubira D, Sekar D. Liquid biopsy: exosomal microRNAs as novel diagnostic and prognostic biomarkers in cancer. Mol Cancer. 2022;21:54.
32. Vajaria BN, Patel PS. Glycosylation: a hallmark of cancer?. Glycoconj J. 2017;34:147–156.
33. Nelson KM, Weiss GJ. MicroRNAs and cancer: past, present, and potential future. Mol Cancer Ther. 2008;7:3655–3660.
34. Berindan-Neagoe I, Monroig Pdel C, Pasculli B, Calin GA. MicroRNAome genome: a treasure for cancer diagnosis and therapy. CA Cancer J Clin. 2014;64:311–336.
35. Garcia-Martin R, Wang G, Brandão BB, Zanotto TM, Shah S, Kumar Patel S, et al. MicroRNA sequence codes for small extracellular vesicle release and cellular retention. Nature. 2022;601:446–451.
36. Chen X, Yu L, Hao K, Yin X, Tu M, Cai L, et al. Fucosylated exosomal miRNAs as promising biomarkers for the diagnosis of early lung adenocarcinoma. Front Oncol. 2022;12:935184.
37. Zhang J, Li S, Li L, Li M, Guo C, Yao J, et al. Exosome and exosomal microRNA: trafficking, sorting, and function. Genom Proteom Bioinform. 2015;13:17–24.
38. Zhao S, Mi Y, Guan B, Zheng B, Wei P, Gu Y, et al. Tumor-derived exosomal miR-934 induces macrophage M2 polarization to promote liver metastasis of colorectal cancer. J Hematol Oncol. 2020;13:156.
39. Sun Z, Ji N, Bi M, Zhang Z, Liu X, Wang Z. Negative expression of PTEN identifies high risk for lymphatic-related metastasis in human esophageal squamous cell carcinoma. Oncol Rep. 2015;33:3024–3032.
40. Lee YR, Chen M, Pandolfi PP. The functions and regulation of the PTEN tumour suppressor: new modes and prospects. Nat Rev Mol Cell Biol. 2018;19:547–562.
41. Zeng Q, Zhu Z, Song L, He Z. Transferred by exosomes-derived MiR-19b-3p targets PTEN to regulate esophageal cancer cell apoptosis, migration and invasion. Biosci Rep. 2020;40:BSR20201858.
42. He L, Zhu W, Chen Q, Yuan Y, Wang Y, Wang J, et al. Ovarian cancer cell-secreted exosomal miR-205 promotes metastasis by inducing angiogenesis. Theranostics. 2019;9:8206–8220.
43. Sun JF, Zhang D, Gao CJ, Zhang YW, Dai QS. Exosome-mediated MiR-155 transfer contributes to hepatocellular carcinoma cell proliferation by targeting PTEN. Med Sci Monit basic Res. 2019;25:218–228.
44. Okkenhaug K, Bilancio A, Farjot G, Priddle H, Sancho S, Peskett E, et al. Impaired B and T cell antigen receptor signaling in p110delta PI 3-kinase mutant mice. Science. 2002;297:1031–1034.
45. Kim SH, Das A, Chai JC, Binas B, Choi MR, Park KS, et al. Transcriptome sequencing wide functional analysis of human mesenchymal stem cells in response to TLR4 ligand. Sci Rep. 2016;6:30311.
46. Liu M, Guo S, Hibbert JM, Jain V, Singh N, Wilson NO, et al. CXCL10/IP-10 in infectious diseases pathogenesis and potential therapeutic implications. Cytokine Growth Factor Rev. 2011;22:121–130.